A numerical and theoretical study of the multipactor appearance in the presence of a DC parallel electric field

Adrien Plaçais, Julien Hillairet, Mohamed Belhaj, Jérôme Puech

AIP Advances

A numerical and theoretical study of the multipactor appearance in the presence of a DC parallel electric field

Cite as: AIP Advances **12**, 025022 (2022); https://doi.org/10.1063/5.0062499
Submitted: 06 July 2021 • Accepted: 01 February 2022 • Published Online: 18 February 2022

A. Plaçais, J. Hillairet, M. Belhaj, et al.

A numerical and theoretical study of the multipactor appearance in the presence of a DC parallel electric field

Cite as: AIP Advances 12, 025022 (2022); doi: 10.1063/5.0062499
Submitted: 6 July 2021 • Accepted: 1 February 2022 •
Published Online: 18 February 2022

A. Plaçais,[1,a] J. Hillairet,[1,b] M. Belhaj,[2,c] and J. Puech[3,d]

AFFILIATIONS

[1] CEA, IRFM, F-13108 Saint-Paul-Lez-Durance, France
[2] DPHY, ONERA, Université de Toulouse, F-31055 Toulouse, France
[3] CNES, DSO/RF/HNO, F-31401 Toulouse, France

[a] **Author to whom correspondence should be addressed:** adrien.placais@lpsc.in2p3.fr. **Also at:** DPHY, ONERA, Université de Toulouse F-31055 Toulouse, France and CNES, DSO/RF/HNO, F-31401 Toulouse, France.
[b] **Electronic mail:** julien.hillairet@cea.fr
[c] **Electronic mail:** mohamed.belhaj@onera.fr
[d] **Electronic mail:** jerome.puech@cnes.fr

ABSTRACT

In this paper, we study the appearance of the multipactor in a simple system with a bottom plate holding a static potential V_d. We developed a numerical model to compute the evolution of the multipactor threshold as a function of the potential. We identify the nature of the resonant modes that appear at different V_d using resonance theory. Then, we use it to compute the theoretical threshold of the structure. As we use a very simplistic electron emission model to identify the multipactor modes, we compute the threshold in a more realistic configuration in a second step.

I. INTRODUCTION

The multipactor effect is a phenomenon appearing in vacuum radio-frequency (RF) devices when two requirements are met: (i) residual electrons in the system enter in resonance with the RF electric field and (ii) their energy is high enough to emit other electrons when impacting the walls. In practice, the multipactor appears when the RF electric field reaches a certain amplitude threshold E_{th}. This phenomenon can degrade the RF signal or partially dissipate the RF power. In the nuclear fusion and space telecommunications fields, the main issue with the multipactor is that it can cause overheating of the surfaces.[1] When the heat flux is large enough, it can lead to outgassing of the surfaces; the ejected matter can ionize, potentially leading to destructive corona breakdowns.[2]

Electron emission phenomena are at the origin of the augmentation in electron population. When an electron called a Primary Electron (PE) impacts a sample, it can emit other electrons. We distinguish three populations of emitted electrons: Secondary Electrons (SEs), which are electrons removed from the material, and Inelastically Backscattered Electrons and Elastically Backscattered Electrons (IBEs, EBEs), which are PEs reflected by the sample, respectively, with and without energy loss.

We characterize these emitted electron populations by three quantities: an energy distribution, an angular distribution, and an emission yield. The emission yield of a population is the ratio between the flux of this population and the flux of PEs. The secondary electron emission yield is noted as SEEY or δ. The inelastically backscattered electron emission yield and the elastically backscattered electron emission yield are, respectively, noted IBEEY, η_i and EBEEY, η_e. These quantities mainly rely on the nature of the sample and surface state and on the energy and direction of the flux of PEs. We define the Total Electron Emission Yield (TEEY) as

$$\sigma \equiv \delta + \eta_e + \eta_i. \quad (1)$$

This quantity is of the utmost importance, as $\sigma > 1$ conveys an increase in the electron population and is one of the necessary conditions for multipacting. This is not a multipactor appearance sufficient condition as it does not guarantee that the electron cloud enters in resonance with the RF signal.

The multipactor appearance mechanisms are well understood in simple configurations, such as rectangular or coaxial metallic waveguides, for which the multipactor susceptibility chart is commonly employed. However, multipacting predictability becomes less reliable in several situations, including RF devices with complex geometries and RF devices involving a magnetic field.[3,4] In particular, dielectric materials are of primordial interest in modern RF applications. Unlike metals, they can hold a net electric charge, which influences both their emission properties[5] and the RF signal/electron resonance.[6,7] Thus, these materials strongly complicate the appearance of the multipactor. In addition, the charge trapped at the surface of dielectric is not uniform[8] and evolves with each electron collision. In this study, we focus on the influence of dielectrics on resonance mechanisms; we model charged dielectrics materials by a DC electric field.

The rest of this paper is organized as follows: In Sec. II, we use the numerical tool POTOMAC to compute the multipactor threshold E_{th} of a parallel-plate waveguide as a function of the potential of the bottom plate. The electron emission model is voluntarily kept very simple. As the chart $E_{\text{th}}(V_d)$ shows distinct regimes, we develop, in Sec. III, a resonance theory to study these regimes, which is solvable with the very simple electron emission model. In Sec. IV, we compare electrons emission phase calculated with POTOMAC with emission phases obtained with the resonance theory. In Sec. V, we compute the multipactor thresholds with the resonance theory in order to compare them with the thresholds calculated with POTOMAC. Finally, in Sec. VI, we make a second set of POTOMAC simulations with a more realistic electron emission model, to study its influence on the multipactor appearance.

II. NUMERICAL STUDY

A. Presentation of the model

The system under study, illustrated in Fig. 1, is composed of two parallel metallic plates, infinite in the $\hat{\mathbf{y}}$ and $\hat{\mathbf{z}}$ directions. The plates are separated by a gap of length d. The RF electric field $\mathbf{E}_{\text{RF}}$ has an amplitude E_0, a frequency f, and is oriented along $\hat{\mathbf{x}}$,

$$\mathbf{E}_{\text{RF}}(t) = E_0 \sin(\phi)\hat{\mathbf{x}}, \quad (2)$$

with the phase $\phi = 2\pi ft$, where t is the time. The model is in 1D, and electrons move along $\hat{\mathbf{x}}$. The origin of coordinates is set on the bottom plate. The motion of electrons is non-relativistic. The bottom plate is maintained at a potential V_d, whereas the top plate is grounded. The voltage difference between the plates creates a static and uniform electric field $\mathbf{E}_{\text{d}}$, oriented along $\hat{\mathbf{x}}$. Their charge is static, uniform, and does not affect electron emission phenomena.

As the electron emission model and its parameters have a tremendous influence on the calculated multipactor threshold,[9] we use the same emission model for simulation and theory. Yet, the main assumption underlying resonance theory is that all electrons participating to the growth of the electron cloud follow the same trajectory. This hypothesis forbids the use of energy and angular distributions for emitted electrons. Hence, we use a naive electron emission model; all electrons are emitted with the same constant energy and there is no EBE. SEs and IBEs are not discriminated from each other. The SEEY is computed from Dionne model as defined in Ref. 10. The model is summarized in Table I.

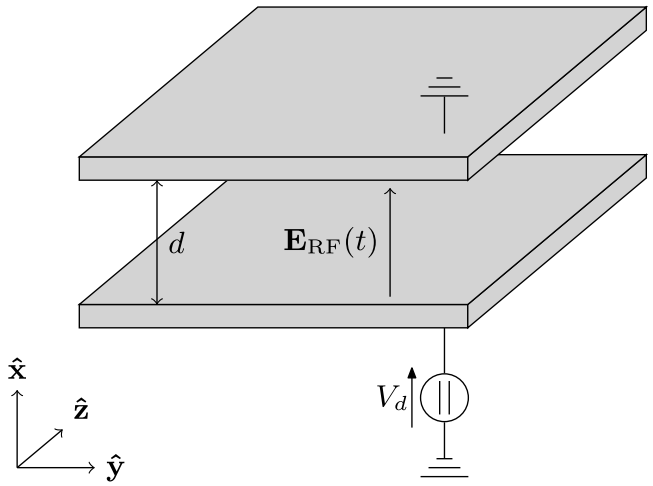

FIG. 1. Infinite parallel plates separated by a distance d. Potential of the bottom plate is V_d, the top plate being maintained at ground potential. A uniform RF electric field $\mathbf{E}_{\text{RF}}$ propagates between the plates.

TABLE I. Full electron emission model used in this study. There is no model for EBEs, as they are not considered here.

Population	Emission yield	Angular distrib.	Energy distrib.
SE	Dionne model	No (1D)	Monoenergetic
IBE	Constant	No (1D)	Monoenergetic
EBE			

For the sake of simplification, we consider that the metallic plates have the same emission properties and that $V_d \geq 0$ V. For symmetry reasons, this study and all its conclusions are still valid with a negative potential. In addition, we can easily adapt it to configurations where the plates have different emission properties.

B. Presentation of the numerical tool POTOMAC

POTOMAC (Physical simulatiOn TOol for Multipactor in Advanced Configurations) is a physical Electro-Static Particle-in-Cell (ES-PIC) code that models the multipactor appearance and, in particular, compute the multipactor threshold of a structure. It is possible to simulate configurations involving dielectric materials and/or magnetic fields.[11,12] N_e seed electrons are injected in the waveguide during the three first signal periods. The simulation is carried on for up to 60 000 periods. If the number of electrons goes higher than $5N_e$, the multipactor is found and the simulation stops. If it drops below $N_e/10$ or if the end of simulation is reached, simulation restarts with a higher E_0. We found this criterion to be more robust than the detection of an exponential growth of the electron

population. As a matter of a fact, this last one led to premature detection of the multipactor at very low electric fields, caused by temporary increase in electron population. As we are only interested in the multipactor threshold determination, space charge effects are neglected.[1] Such approximation would be, of course, too strong to study the multipactor evolution in an established regime.[13,14]

The electron positions and velocities are calculated with a leapfrog scheme. In PIC codes, the time step Δt has a tremendous importance. In general, two conditions have to be matched,[15]

$$\begin{cases} \Delta t \ll 1/f, & \text{(3a)} \\ \Delta t < \Delta x / v_{\max.} & \text{(3b)} \end{cases}$$

Δx is the spatial step. v_{th} is the velocity of the most energetic electrons appearing in the system; its value depends on the geometry under study. The pseudo-random numbers generator is a Tausworthe generator:[16] it has a period and is uniform. At each collision, σ is calculated. The number of electrons emitted is an integer calculated with a Poisson distribution.[17] When only one electron is emitted, it has a probability η_e/σ to be an EBE, a probability η_i/σ to be an IBE, and a probability δ/σ to be a SE. When many electrons are emitted, they are always SEs.[17,18]

We implemented numerical diagnostic tools in POTOMAC. They make it possible to register several internal parameters, such as the nature (seed, SE, EBE, IBE) of every electron and of the electron that emitted them. In this paper, we utilize it to record the emission phase, the collision phase, the emission plate, and the collision plate of every simulated electron for every potential V_d at the multipactor threshold E_{th}.

C. POTOMAC simulation results

In this study, we consider $d = 0.1$ mm, and the RF electric field has a frequency of 11 GHz. We sweep the RF electric field amplitude between 4.3 and 15 kV cm^{-1}. The material is copper *as received* (without any surface treatment), which TEEY was measured at the ONERA. Experimental data can be found in Ref. 19 and details on the measurements in Ref. 10. The TEEY, as a function of the impact energy of PEs, is represented in Fig. 2. The first cross-over energy, defined as the first energy for which $\sigma = 1$, is $E_{c,1} = 29$ eV. The list of the electron emission model parameters is presented in Table II. All electrons are emitted with the same energy of 3 eV.

We take $\Delta x = d/100$ and $N_e = 100$. We showed in another paper[10] that, with POTOMAC and in this geometry, most energetic electrons had an energy of 300 eV. The Δt value matching conditions (3a) and (3b) in these conditions were set to $\Delta t = T_{\text{RF}}/1000$, where T_{RF} is the period of the signal. We verified the consistency of POTOMAC's results with other simulation codes and multipactor theories, as well as its convergence. A consistency study in a simple configuration is presented in the Appendix, as well as a convergence study on the initial number of electrons.

Figure 3 represents the evolution of E_{th} with V_d, as calculated with POTOMAC. Four regions of potentials are visible:

- zone 1 ($V_d = 0$–19.3 V), where E_{th} increases with V_d in a parabola-like shape.
- zone 2 ($V_d = 19.3$–26.5 V), where E_{th} slowly decreases with V_d.

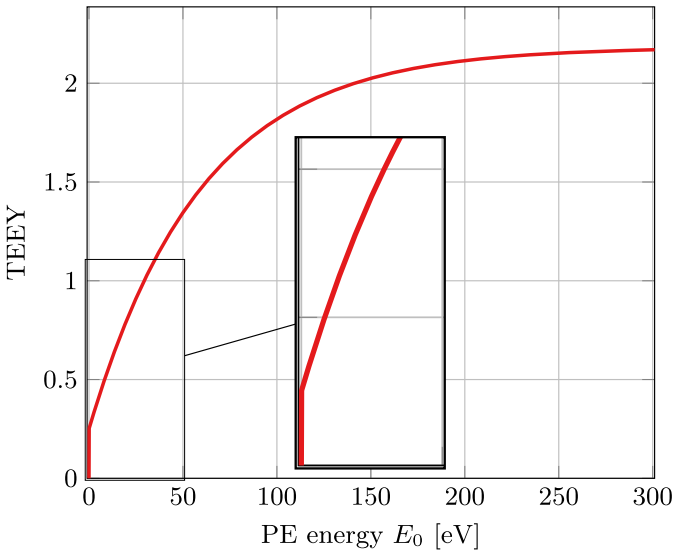

FIG. 2. Modeled TEEY as a function of the impact energy of PEs used in this study.

TABLE II. Copper Dionne's parameters as defined in Ref. 10.

Parameter	Value
A	12.48
n	1.00
d (nm)	4.80
S	0.15
Φ (eV)	4.65
η_i	0.25

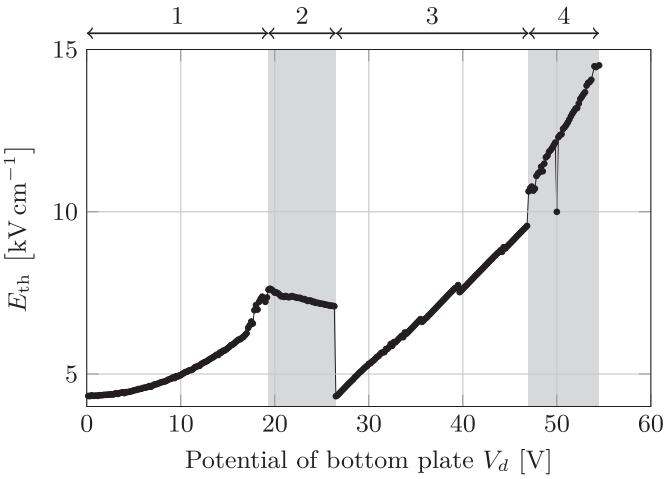

FIG. 3. The evolution of the multipactor threshold with the potential at the surface of the bottom plate.

- zone 3 (V_d = 26.5–47.0 V), where E_{th} drops by 39% and then linearly increases with V_d.
- zone 4 (V_d = 47.0–54.5 V). At 47 V, E_{th} is abruptly raised by 11%. Then, it linearly increases with V_d.

The isolated point at V_d = 50 V is not reproducible, and it corresponds to a case where a significant number of seed electrons were injected in resonance with the RF electric field, leading to a very rapid increase in electron density. For V_d > 54.5 V, the multipactor threshold dramatically increases. As RF systems have transmissible power limitations, we can then consider that the multipactor disappears.

D. Comparison with previous studies

Sorolla *et al.*[6] computed the multipactor threshold of an infinite parallel-plate dielectric-loaded system with a numerical model in 1D. They took into account the evolution of the dielectric slab charge with each electron collision, as well as the influence of this charge on the SEEY.[5] They kept the charge relatively low, corresponding to our zone 1. In this zone, the shape of our threshold vs charge curves are similar.

Zhai *et al.*[7] studied the evolution of E_{th} with V_d in a parallel-plate dielectric-loaded waveguide. Their simulation is 1D. They used Vaughan model to compute the TEEY,[20,21] and all electrons were emitted with an energy of 3.68 eV. Although the general shape of their $E_{\text{th}}(V_d)$ curve (Fig. 4) is similar to ours, they did not observe the strong discontinuities at 26.5 and 47.0 V. They are unphysical and are created by the lack of dispersion in electrons impact velocities, compelling all electrons to enter in the same multipactor mode. We believe that Zhai *et al.* did not observe these because they allowed the dielectric charge to vary, smoothing the transitions between modes. According to their hypothesis, the multipactor is in a Double-Sided (DS) mode at low potential and progressively switches to a Single-Sided (SS) mode when the potential difference between the plates increases. In a DS mode, the multipactor is created by electrons impacting a plate different from their emission plate. In a SS mode, it is created by electrons impacting their emission plate.

In order to verify these conclusions and validate POTOMAC simulation results, in Sec. III, we develop a multipactor resonance theory adapted to this configuration.

III. DEVELOPMENT OF THE RESONANCE THEORY

A. Motion equations and notations

In this section, we investigate the multipactor resonant trajectories and resonant phases, regardless of electrons impact energies. All electrons have a mass m and a charge $-|e|$. They have a low energy (some keV at most); thus, their motion is non-relativistic, and we can neglect the RF magnetic field.[22] We use the dimensionless set of equations proposed by Sorolla *et al.*,[6]

$$\begin{cases} \Lambda \equiv \dfrac{m\omega^2}{|e|E_0} \cdot x, & \text{(4a)} \\ V_\omega \equiv \dfrac{m\omega}{|e|E_0} \cdot v_x, & \text{(4b)} \\ \Omega \equiv \dfrac{E_d}{E_0}. & \text{(4c)} \end{cases}$$

The dimensionless position is Λ, and the dimensioned position is x. The dimensionless velocity is V_ω, and the dimensioned velocity is v_x.

We set the origin of positions on the bottom plate, which is therefore at the position Λ = 0. The top plate is at Λ_d. All electrons emitted from the bottom plate have an initial velocity $V_{\omega,0}$, and those emitted from the top plate have an initial velocity $-V_{\omega,0}$. The motion equations for an electron emitted at ϕ_1 at the position Λ_1 with the velocity $V_{\omega,1}$ are as follows:[6]

$$\begin{cases} V_\omega = \cos\phi - \cos\phi_1 - \Omega(\phi - \phi_1) + V_{\omega,1}, & \text{(5a)} \\ \Lambda = (\phi - \phi_1)(V_{\omega,1} - \cos\phi_1) + \sin\phi - \sin\phi_1, \\ \quad - \dfrac{\Omega}{2}(\phi - \phi_1)^2 + \Lambda_1. & \text{(5b)} \end{cases}$$

We call *crossing electrons* as electrons that are emitted on the bottom plate and impact the top plate (short form: b → t) and electrons that are emitted on the top plate and impact the bottom plate (short form: t → b). Similarly, we call *recollected electrons* as electrons emitted on the bottom plate and impact the bottom plate (b → b), and electrons emitted on the top plate and return to it (t → t). Due to the positive potential on the bottom plate, t → t electrons cannot enter in resonance with the RF electric field, though individual t → t electrons can exist. Without any loss of generality, we consider that the first resonant trajectory always starts on the bottom plate.

We consider an electron emitted at the phase ϕ_k, with k an integer different from zero. It impacts a plate (the same or another one) at the phase ϕ_{k+1}. The time between the collision of a PE and the emission of the electrons is in the range 10^{-11}–10^{-12} s,[23] which is at least two orders of magnitude lower than the period of a GHz signal. Thus, we consider that the electron emission phenomena are instantaneous. As a consequence, ϕ_k is also the collision phase of the precedent electron and ϕ_{k+1} the emission phase of the next electron. Riyopoulos *et al.*[24] showed that making this hypothesis had little influence on the resonance mechanisms.

The DS multipactor is created by crossing electrons. The classic DS multipactor resonance condition reads[1,25]

$$\phi_2 = \phi_1 + N\pi, \quad N = 1, 3, 5, \ldots, \tag{6}$$

with N the multipactor order. The solid lines in Fig. 5 represent the trajectories of two electrons between two grounded plates. The first one checks the resonance condition (6). As V_d = 0 V, the second electron also checks this condition and resonance is ensured. The dashed lines in Fig. 5 represent the trajectories of two electrons, the bottom plate being set to V_d = 10 V. The first electron checks the resonance condition (6). The positive potential on the bottom plate breaks the symmetry of the problem, and the second electron is out of resonance.

B. Asymmetric multipactor modes

In the asymmetric multipactor modes, the multipactor involves n_φ = 1, 2, 3, ... different resonant trajectories. The kth electron is emitted at the phase ϕ_k on the plate whose position is Λ_k, with an initial velocity $V_{\omega,k}$. It impacts the plate of position Λ_{k+1} at the phase ϕ_{k+1}. We define the multipactor period Π,

$$\Pi = \phi_{n_\varphi+1} - \phi_1. \tag{7}$$

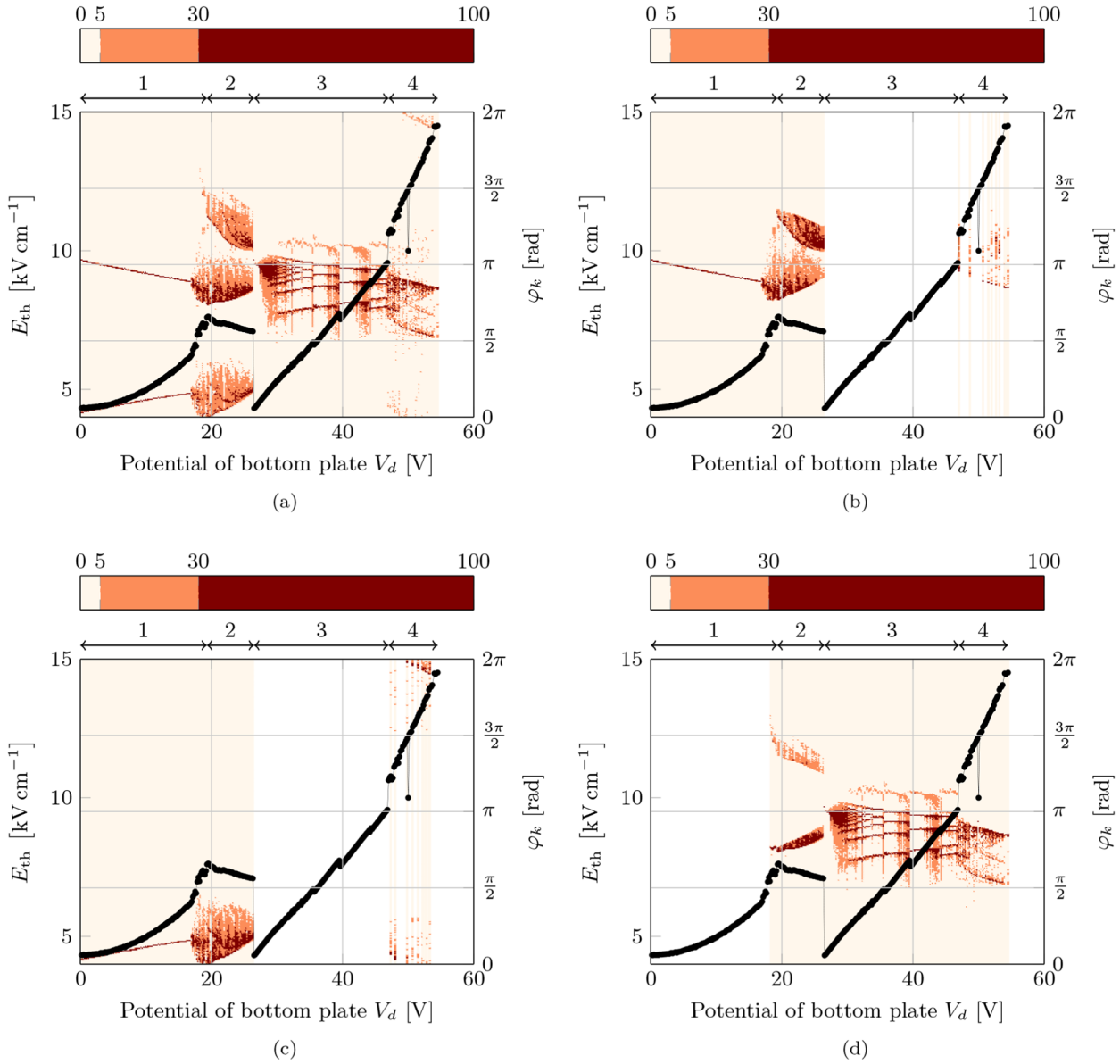

FIG. 4. The multipactor threshold calculated by POTOMAC as a function of V_d (left axis, —●—). The evolution of the electrons emission phase distribution with V_d, extracted from POTOMAC simulations (right axis, ◢). Electrons are sorted depending on their trajectories: (a) all electrons, (b) b → t electrons, (c) t → b electrons, and (d) b → b electrons.

We define the resonant or fixed phases,

$$\varphi_k \equiv mod\,(\phi_k, \Pi), \quad k = 1, 2, 3, \ldots. \tag{8}$$

The sequence of resonant phases $(\varphi_1, \varphi_2, \ldots, \varphi_{n_\varphi})$ is repeated every Π.

We name asymmetric DS[26] and SS modes by the subset (Π, n_φ). For example, the symmetric multipactor resonance mechanism presented in Fig. 5 is called DS $(\Pi = \pi, n_\varphi = 1)$. We represented in Fig. 6 the seven resonant trajectories of the SS $(\Pi = 12\pi, n_\varphi = 7)$.

The ping-pong modes involve both crossing and recollected electrons.[27,28] In order to completely characterize these modes, we should provide the list and ordering of the impacted plates. We use the notation $x_1 \to x_2 \to \cdots \to x_{n_\varphi}$, where x_k is "b" if the kth electron is emitted on the bottom plate and "t" if it is emitted on the top plate. We present in Fig. 7 the trajectories of the PP $(\Pi = 4\pi, n_\varphi = 3)$ b → t → b.

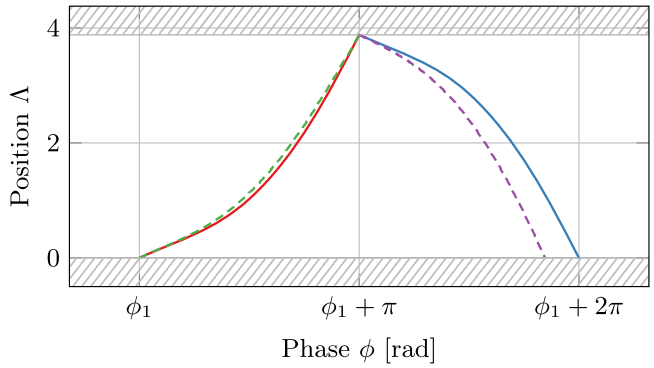

FIG. 5. Solid lines: resonant trajectory of the two first electrons in the symmetric first order DS mode, with V_d = 0 V, ϕ_1 = 2.73 rad, and E_0 = 7.00 kV cm^{-1}. Dashed lines: trajectory of two electrons, the first one checks (6), with V_d = 10 V, ϕ_1 = 2.98 rad, and E_0 = 7.00 kV cm^{-1}.

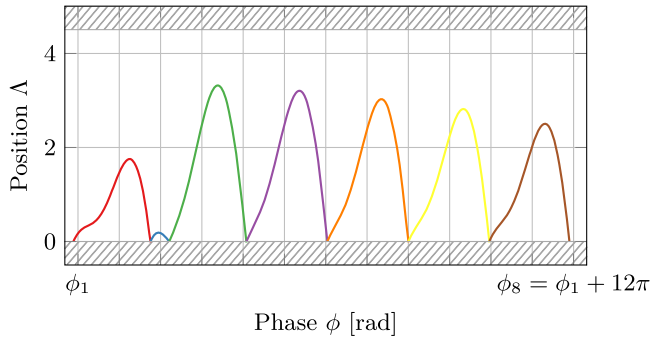

FIG. 6. Trajectory of the electrons in the SS ($\Pi = 12\pi, n_\varphi = 7$). V_d = 33.0 V, ϕ_1 = 2.650 rad, and E_0 = 6.03 kV cm^{-1}.

C. Method of resolution

In a fashion similar to the symmetric case and for a given Ω, we solve the n_φ position equations, the unknowns being the phases ϕ_k,

$$\begin{aligned}\Lambda_{k+1} = {} & (\phi_{k+1} - \phi_k)(V_{\omega,k} - \cos\phi_k) \\ & + \sin\phi_{k+1} - \sin\phi_k \\ & - \frac{\Omega}{2}(\phi_{k+1} - \phi_k)^2 + \Lambda_k, \quad k = 1, 2, \ldots, n_\varphi. \end{aligned} \tag{9}$$

The number of phases n_φ, the values of Λ_k, $V_{\omega,k}$, and of $\phi_{n_\varphi+1} - \phi_1$ are set by the multipactor mode under study. We solve this system numerically; we used a least-squares algorithm.[29,30]

We set up some additional constraints to ensure the convergence and physicality of the results. We impose $\phi_{k+1} - \phi_k > 2\pi/100$ to avoid electrons being recollected at the same time they are emitted. We also force $\phi_1 \in [0, 2\pi]$. Finally, we impose $\Lambda(\phi) \in [0; \Lambda_d]$ to forbid the premature impact of an electron on the *wrong* plate, such as a b → t electron going through negative values of position before impacting the top plate.

The multipactor can only appear, thanks to the *phase-focusing* effect, when a small deviation in the electron emission phase leads to a smaller deviation of its collision phase. Then, the mode is said to be stable. This condition can be written as[26]

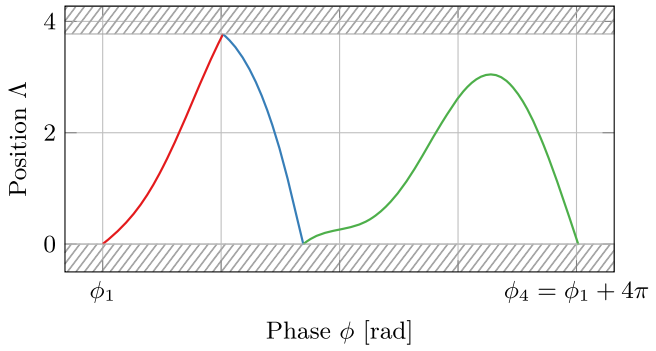

FIG. 7. Trajectory of the electrons in the PP ($\Pi = 4\pi, n_\varphi = 3$) b → t → b. V_d = 25.00 V, ϕ_1 = 3.52 rad, and E_0 = 7.21 kV cm^{-1}.

$$\left|\frac{\delta\phi_{n_\varphi}}{\delta\phi_1}\right| = \left|\frac{\delta\phi_2}{\delta\phi_1} \cdot \frac{\delta\phi_3}{\delta\phi_2} \cdots \frac{\delta\phi_{n_\varphi}}{\delta\phi_{n_\varphi-1}}\right| < 1. \tag{10}$$

IV. EMISSION PHASE STUDY

For every potential V_d and at the multipactor threshold, we recorded the emission and collision phase as well as the emission and collision plate of every simulated electron (cf. Subsection II B). Emission phases are represented as heatmaps to show their evolution with V_d and are represented in the range $[0, 2\pi]$. In Figs. 7(b)–7(d), we represented the distribution of all the emission phases of all electrons. In Figs. 7(b)–7(d), we represented the emission phases of electrons according to their trajectory: b → t, t → b, and b → b. We did not represent t → t electrons as their number is always negligible or null.

Each emission phase distribution was normalized between 0 and 100, and color bars were chosen so as to discern three types of emission phases:

- phases where a negligible number of electrons were emitted (noise);
- phases where a relatively small number of electrons were emitted; and
- phases where a relatively high number of electrons were emitted.

In order to compare these heatmaps to the resonance theory, we calculated the resonant phases of every relevant multipactor mode for every potential V_d (cf. Subsection III C). $\Omega = E_{\text{th}}/V_d$ is calculated with the POTOMAC thresholds presented in Subsection II C (Fig. 3 results).

A. Zone 1

In this zone, there are no b → b electrons; hence, the multipactor is created by DS dynamics. Here, the only relevant mode is the DS ($\Pi = 2\pi, n_\varphi = 2$), and the emission phases are represented in Fig. 8. We observed that equations of higher order and/or higher period multipactor did not have any solution in this configuration. The DS ($\Pi = 2\pi, n_\varphi = 2$) admits two solutions: the first one is perfectly matching POTOMAC data, and the second solution is unstable.[1] Around V_d = 18 V, POTOMAC emission phases start to scatter, even if they remain close to the theoretical phases.

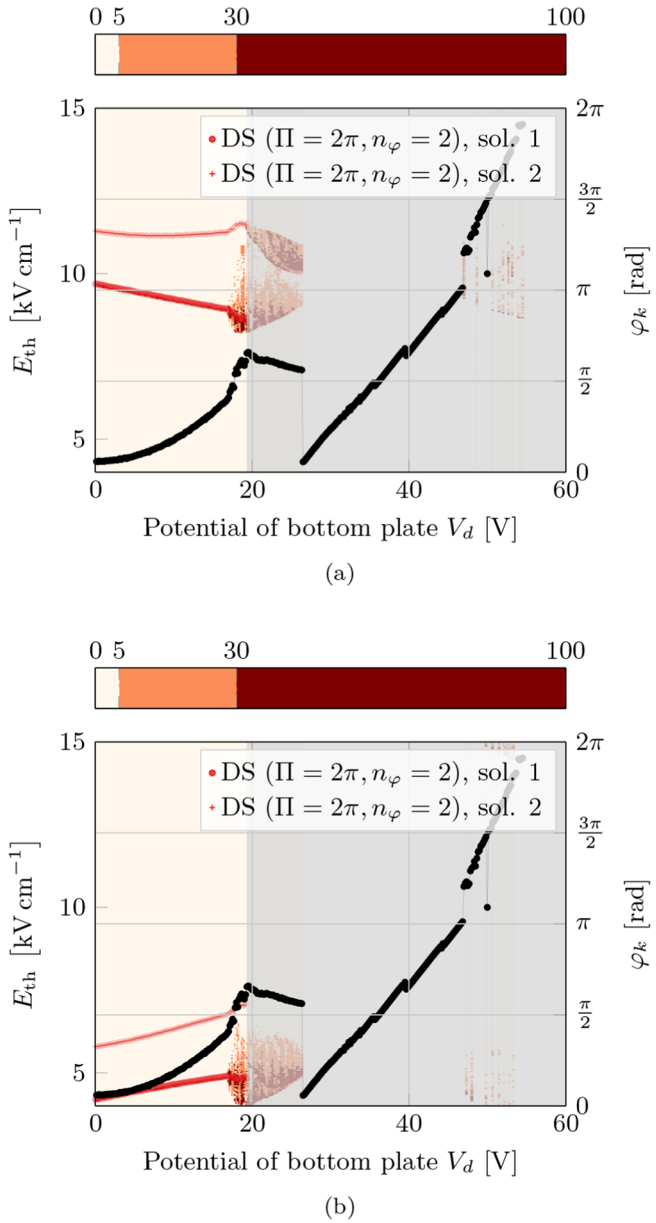

FIG. 8. The multipactor threshold calculated by POTOMAC as a function of V_d (left axis, —●—). The evolution of the crossing electrons emission phase distribution with V_d, extracted from POTOMAC simulations (right axis, ◢) and for various modes. Electrons are sorted depending on their trajectories: (a) b → t electrons and (b) t → b electrons.

B. Zone 2

Emission phases are scattered in zone 2; thus, the multipactor is created by non-resonant dynamics. As there is no finite suite of fixed phases $(\varphi_1, \varphi_2, \ldots, \varphi_{n_\varphi})$, this multipactor cannot be described by resonant theory.

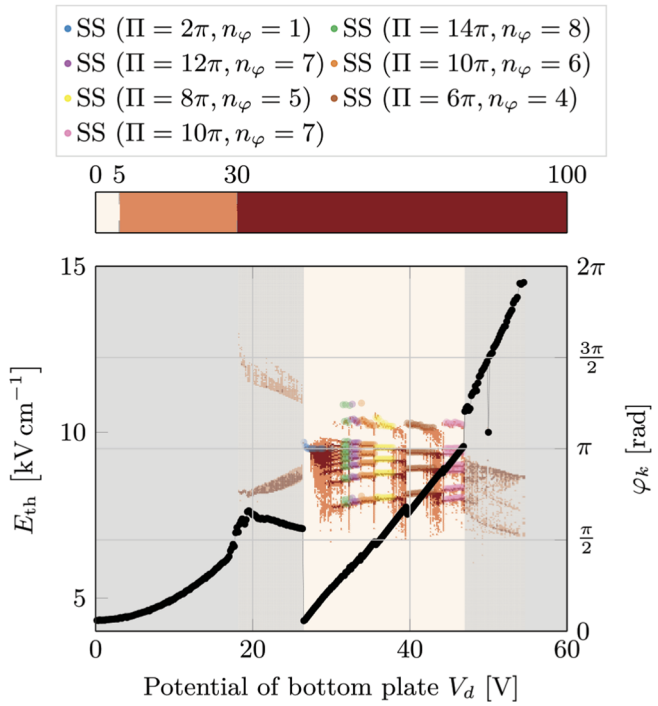

FIG. 9. The multipactor threshold calculated by POTOMAC as a function of V_d (left axis, —●—). The evolution of the b → b electrons emission phase distribution with V_d, extracted from POTOMAC simulations (right axis, ◢) and for various modes.

C. Zone 3

E_{th} drops by 39% at the transition between 2 and 3, which is correlated with a sharp change in the emission phases. It translates the passage of a V_d threshold after which SS dynamics can appear. We represented in Fig. 9 this zone relevant modes. Between 26.5 and 27 V, the SS ($\Pi = 2\pi, n_\varphi = 1$) theoretical emission phases correspond to emission phases calculated by POTOMAC. From 27 V and up to 31.5 V, they scatter, and we cannot discern delimited phases. Increasing the number of initial electrons would solve this issue as it would increase the resolution of the heatmap. It would, however, drastically increase the computation time.

Around 31.5 V and above, we observe separated emission phases corresponding to various SS modes, summarized in Table III. The highest emission phase of all these modes (around 3.6 rad) is barely visible on the heatmap. As a matter of fact, a multipactor mode with several resonant trajectories is likely to involve collisions with a TEEY inferior to unity, resulting in a temporary decrease in electron density. As an example, Table IV shows the emission phases and TEEYs of the SS ($\Pi = 12\pi, n_\varphi = 7$) collisions, for $V_d = 33$ V. We write σ_k the TEEY of the kth collision occurring at ϕ_{k+1}. We can observe that σ_2 is particularly low. Thus, very few electrons are emitted at the phase ϕ_3, and it is nearly invisible in the heatmap. Each mode transition appears chaotic as the emission phases scatter.

D. Zone 4

At the transition between zones 3 and 4, E_{th} significantly increases by 11%. As in zone 2, the emission phases computed by

TABLE III. The single-sided modes found to re-appear in zone 3 with the range of potentials on which they match POTOMAC data.

SS mode	V_d range (V)
$(\Pi = 2\pi, n_\varphi = 1)$	[26.5; 27.0]
$(\Pi = 14\pi, n_\varphi = 8)$	[31.5; 32.3]
$(\Pi = 12\pi, n_\varphi = 7)$	[32.5; 33.5]
$(\Pi = 10\pi, n_\varphi = 6)$	[33.7; 35.5]
$(\Pi = 8\pi, n_\varphi = 5)$	[35.7; 37.8]
$(\Pi = 6\pi, n_\varphi = 4)$	[39.7; 43.0]
$(\Pi = 10\pi, n_\varphi = 7)$	[44.5; 46.8]

TABLE IV. TEEY of the collisions in the SS $(\Pi = 12\pi, n_\varphi = 7)$. V_d = 33.0 V and E_0 = 6.03 kV cm^{-1}. These parameters are identical to those used in Fig. 5.

k	$\mathrm{mod}(\phi_k, 2\pi)$ (rad)	σ_k
1	2.650	1.10
2	2.238	0.28
3	3.661	1.31
4	3.250	1.33
5	3.121	1.33
6	3.011	1.31
7	2.882	1.27

POTOMAC are scattered. The resonance theory cannot describe this configuration, and we did not find any solution matching POTOMAC data.

V. THEORETICAL MULTIPACTOR THRESHOLD

A. Methodology

In Sec. IV, we used the resonance theory to find which multipactor mode appeared at each potential. We injected Ω calculated with POTOMAC in the position equations. In this section, the theoretical multipactor threshold of the structure is calculated without using any data calculated by POTOMAC.

For a period-Π multipactor with n_φ fixed phases, the multipactor will appear if

$$\prod_{k=1}^{n_\varphi} \sigma_k > 1. \tag{11}$$

E_0 is incremented from 4 to 17 kV m^{-1} with 121 steps, and V_d is swept from 0 to 60 V with 101 steps. For a couple (E_0, V_d), the resonant phases of the mode under study (cf. Subsection III C) are calculated. We inject these phases in Eq. (5a) to compute the TEEY of each collision and verify if (11) is fulfilled. If it is not, E_0 is incremented. Otherwise, the threshold is found, and the next potential is studied.

The convergence of every solution was checked. Their stability was verified [Eq. (10)], with the numerical value $\delta\phi_1 = 10^{-2}$ rad. As the stability results can rely on the value of $\delta\phi_1$,[31,32] we tried various values ranging from 10^{-3} to 10^{-1} rad, with no appreciable effect. The multipactor modes presented in Sec. IV, as well as the SS $(\Pi = 2\pi, n_\varphi = 2)$ and the PP $(\Pi = 4\pi, n_\varphi = 3)$ b → t → b, were studied. At a given V_d, several modes can have a solution, and each mode can have several solutions. In this case, we consider that the solution with the lowest threshold is the most *favored* or fundamental, as it would be the first to appear when increasing the RF electric field amplitude.

B. Calculated theoretical multipactor thresholds

In Fig. 10, we present the evolution of E_{th} as calculated by POTOMAC with V_d. We also show the theoretical multipactor thresholds. In general, there is a good matching between these two curves. This is particularly true in the zones 1 and 3, where the modes at the origin of the multipactor were clearly identified in Sec. IV.

In zone 1, the theoretical threshold of the DS $(\Pi = 2\pi, n_\varphi = 2)$ matches the threshold calculated by POTOMAC. This mode is stable, and the relative error between the thresholds is under 2% at 0–16.8 V. At 16.8–19.3 V, where POTOMAC emission phases scatter, this modes becomes unstable and the error grows up to 9%. This instability does not prevent the multipactor from appearing; it leads to an important loss of electrons, compensated by higher impact energies.[33]

In zone 2, the DS $(\Pi = 2\pi, n_\varphi = 2)$ is the most favored between 19.3 and 22.2 V. It is unstable on this range of potentials. The threshold calculated by POTOMAC is underestimated at 19.3–21 V; in this range, the loss of electrons is too important to be compensated by the higher impact velocities. Thus, the non-resonant multipactor occurs, with a slightly higher threshold. At 22.2–26.5 V, the PP $(\Pi = 4\pi, n_\varphi = 3)$ b → t → b has the lowest threshold. It is stable on this whole range. Even if the multipactor is chaotic, we believe

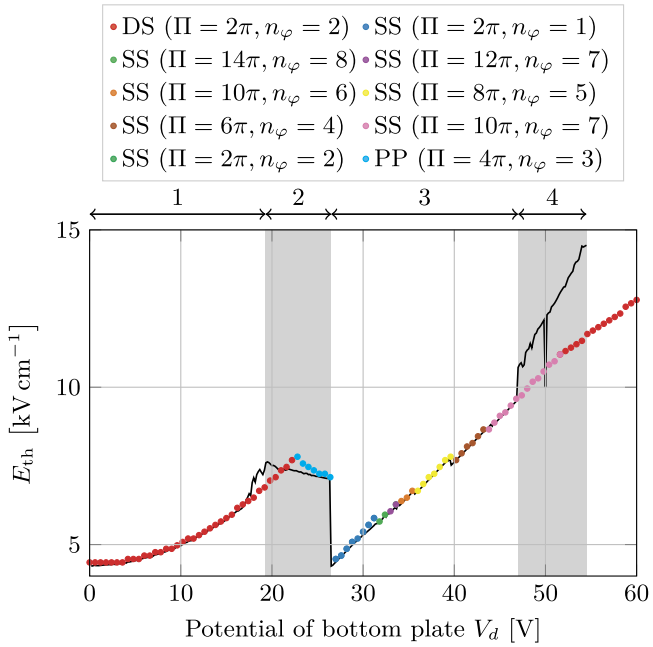

FIG. 10. The evolution of the multipactor threshold calculated by POTOMAC (——) with V_d. The evolution of the theoretical threshold of the most favored mode, for each potential.

that the resonant trajectories of the DS ($\Pi = 2\pi, n_\varphi = 2$) and the PP ($\Pi = 4\pi, n_\varphi = 3$) b → t → b are good approximations of the real electrons trajectories.

In zone 3, the nature and threshold of the modes are consistent with that discussed in Sec. IV. Their error stays under 5%, and they are all unstable. According to Semenov *et al.*,[34] for SS modes, the increase in deviation $\delta\phi_k$ saturates and turns into finite oscillations.

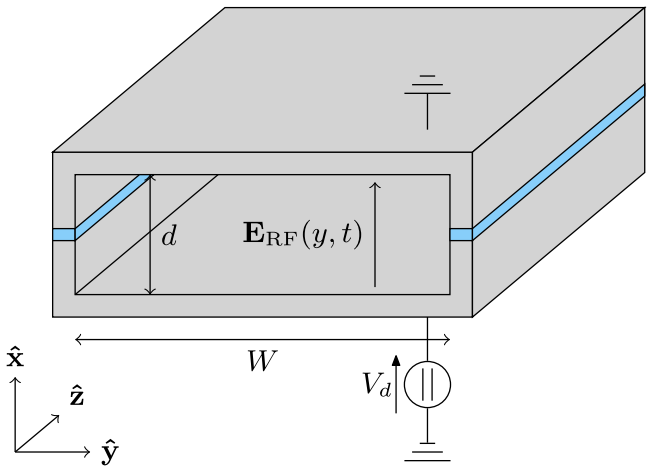

FIG. 11. Infinite metallic rectangular waveguide with a gap d and a width W. Insulating inserts (in blue) isolate the bottom plate from the top plate. They do not influence the $TE_{1,0}$ propagation of $\mathbf{E}_{RF}$. The potential of the bottom plate is V_d, the top plate being maintained at ground potential.

TABLE V. Full electron emission model used in this study.

Population	Emission yield	Angular distrib.	Energy distrib.
SE	Dionne[10]	Cosine law[36]	Chung and Everhart[37]
EBE	SLAB[38]	SLAB[38]	Monoenergetic
IBE	Constant	Cosine law[36]	Uniform

TABLE VI. Copper Dionne's parameters as defined in Ref. 10 for the *more realistic* study.

Parameter	Value
A	6.67
n	1.00
d (nm)	9.47
S	0.14
k_a	0.40
k_b (°)	0.14
Φ (eV)	4.65
η_i	0.25

In zone 4, none of the modes that we studied matches the emission phases calculated by POTOMAC. In particular, the sudden augmentation in E_{th} at 47.0 V is not reproduced by any of the theoretical thresholds.

VI. POTOMAC SIMULATIONS IN 3D, CONSIDERING ENERGY AND ANGULAR DISTRIBUTIONS AS WELL AS EBES

A. Presentation of a more realistic model

We made strong assumptions in the precedent simulations: lack of energy and angular distributions, 1D, and no EBEs. Thus, there was no dispersion in electrons velocity, which created the E_{th} drops

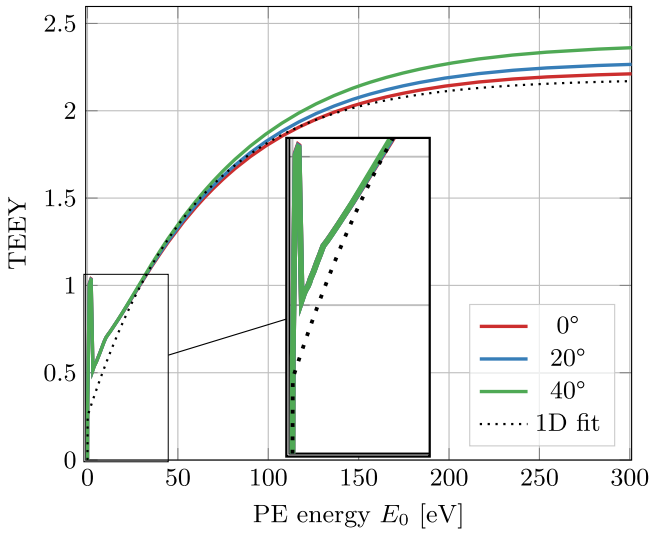

FIG. 12. Modeled TEEY as a function of the impact energy of PEs used in this study. TEEY is represented for various incidence angle θ_0, defined prior to the normal of the sample. The TEEY used in precedent studies is also shown.

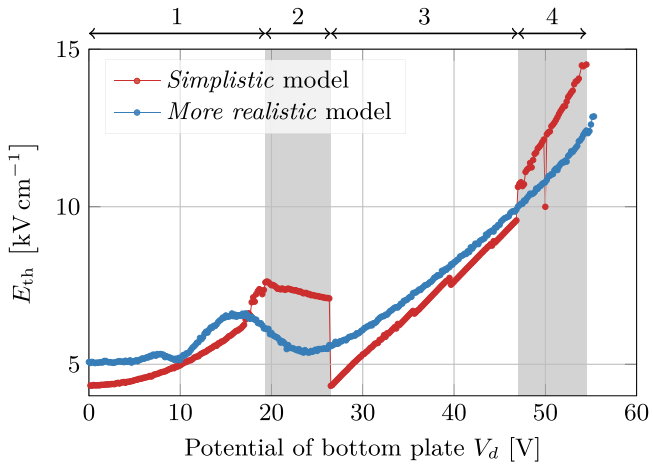

FIG. 13. The multipactor threshold calculated by POTOMAC as a function of the potential on the bottom plate V_d, with the simple and more realistic models.

at 2–3 and 3–4 transitions. In this section, we make POTOMAC simulations in a *more realistic* configuration to study the influence of these hypotheses.

We study in 3D a rectangular waveguide of width $W \gg d$, represented in Fig. 11. The bottom plate is maintained at the potential V_d, while the top plate is grounded. In practice, the insulation can be realized by placing insulating inserts in the waveguide lateral walls. We consider that they do not influence the propagation of the fundamental $TE_{1,0}$ mode,

$$\mathbf{E}_{\mathrm{RF}}(t,y) = E_0 \sin(\phi) \sin\left(\frac{\pi y}{W}\right)\hat{\mathbf{x}}. \tag{12}$$

We neglect the RF magnetic field, which is justified when $W \gg d$.[35] We also neglect the z propagation term of the RF electric field, which comes back to study the (x,y) plane where the electric field amplitude is maximum. The full electron emission model is resumed in Table V.[10] In the remaining part of the paper, we call this new configuration the *more realistic* model, in opposition to the first that was *simplistic*.

For this simulation, we took the closest dimensions possible to the previous dimensions: d = 0.1 mm, W = 19.05 mm, and f = 11 GHz. It corresponds to a WR75 waveguide, with a gap reduced from 9.525 to 0.1 mm. As it is very narrow, the waveguide cannot transmit a significant power and has no industrial

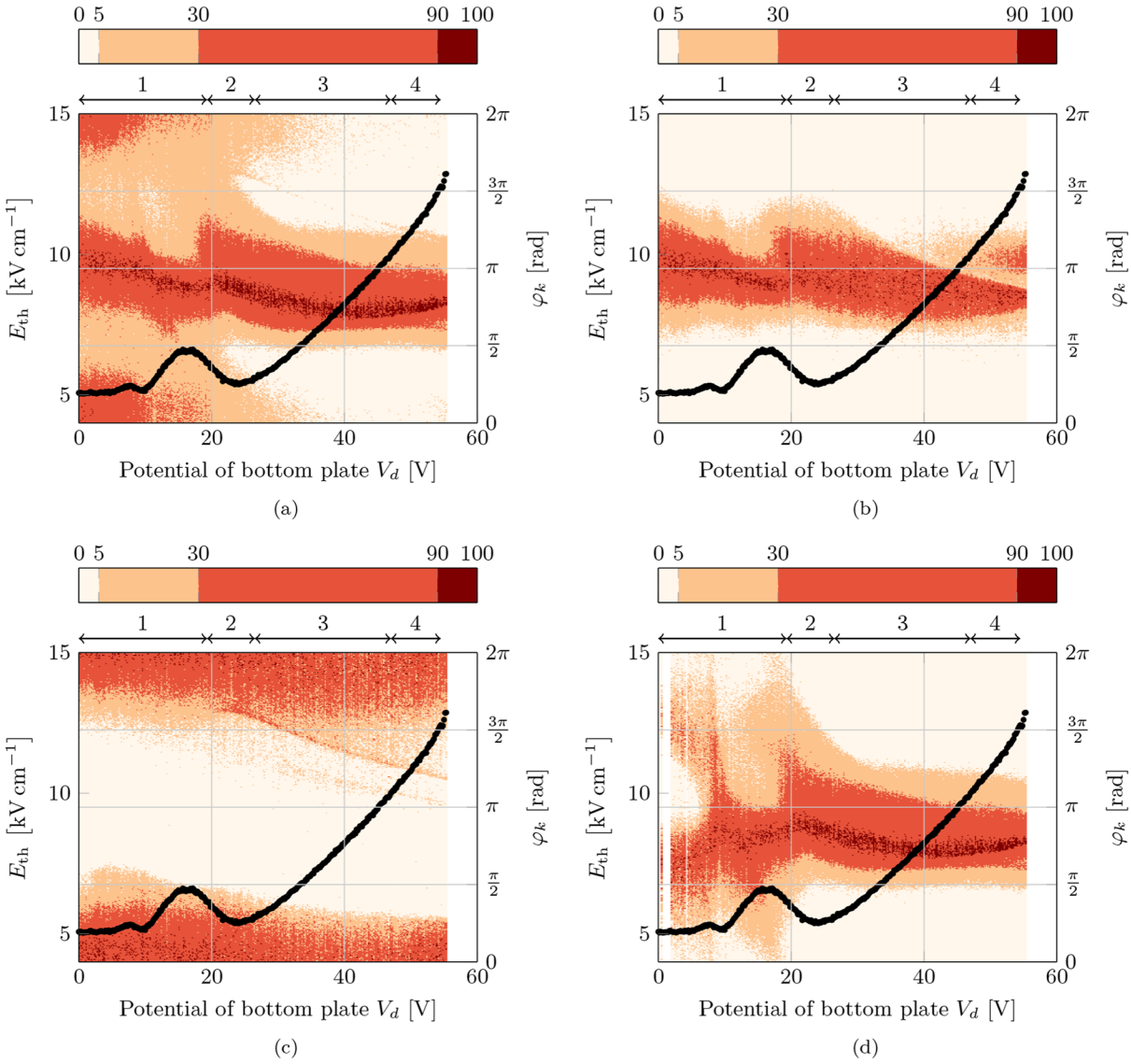

FIG. 14. Heatmaps of electron emission phases in the more realistic configuration. Electrons are sorted depending on their trajectories: (a) all electrons, (b) b → t electrons, (c) t → b electrons, and (d) b → b electrons.

application. However, its very low threshold eases the multipactor measurements. We performed measurements on this system in collaboration with a private company; results will be published in a dedicated article.

In this section, we use a slightly different electron emission model that is in 3D and takes EBEs into account. We fitted the TEEY on the same experimental data as for the first simulation; we reported the model parameters in Table VI. We present in Fig. 12 the TEEY as a function of impact energy; for comparison, we also present the TEEY used in the previous study.

Both fits are similar, except the low-energy peak due to EBEs. New TEEY curve is slightly higher than previous at high energies; we do not expect these differences to be of importance, as the majority of PEs impact walls with a low energy. Here, $E_{c,1}(0^\circ) = 29$ V.

B. Simulation results

We represented in Fig. 13 the evolution of the multipactor threshold with V_d, as calculated by POTOMAC in the two configurations. As a whole, the $E_{\text{th}}(V_d)$ curves are similar in terms of absolute value and general shape. The most notable difference is that the introduction of velocity dispersion erased the strong discontinuities at 26.5 and 47.0 V. In addition, the *more realistic* configuration exhibits a local minimum in threshold at 10 V.

As in Sec. IV, we represented in Fig. 14 electrons emission phase distributions and their evolution with V_d. Each distribution is normalized between 0 and 100. We did not represent t → t, as there is very few of them to contribute to the multipactor. The color bars were chosen so as to discern four main types of emission phases:

- phases where a negligible number of electrons were emitted (noise);
- phases where a relatively small number of electrons were emitted;
- phases where a relatively high number of electrons were emitted; and
- phases where the majority of electrons were emitted, allegedly matching emission phases of *simplistic* model.

As expected, the emission phases are significantly more scattered than in precedent study. Thus, we cannot identify resonant modes as we did earlier in this study. In contrast with the *simplistic* study, there are b → b electrons in zone 1 and crossing electrons in zone 3.

VII. DISCUSSION

We observed that the threshold was always minimum for $V_d = 0$ V. It is to be noted that its position depends on the geometry of the system as well as on the RF frequency. For example, we observed that if we set $d = 0.15$ mm, the minimum was at $V_d = \pm 11$ V. Thus, the results presented in this study should not be generalized. In particular, the addition of a potential difference between the plates does not necessarily raise the threshold.

The resonance theory is based on the strong assumption that all electrons follow the same trajectory; it was shown to be unreasonable when the gap is too big or when the dispersion in emission velocities is too wide.[33,39] In this study, the waveguide is extremely tight, which should not invalid the theory. The main difference between the *simplistic* and the *more realistic* configurations is that we included emission velocities dispersion in the latter. It results on a smoothing of the $E_{\text{th}}(V_d)$ curve, but does not fundamentally change its shape. However, it would be incorrect to assume that, in this configuration, velocity dispersion should be neglected.

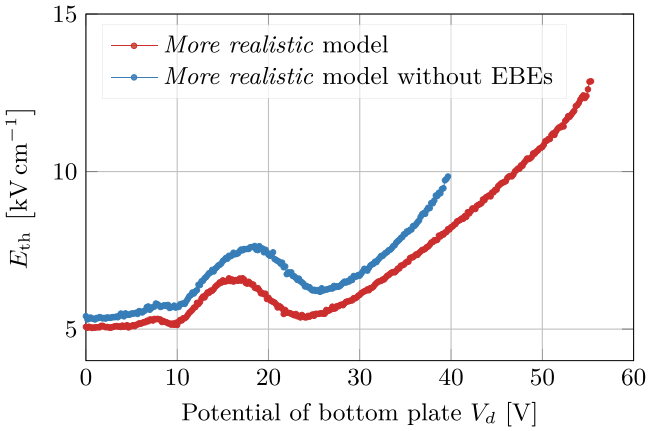

FIG. 15. The multipactor threshold calculated by POTOMAC as a function of the potential on the bottom plate V_d. Threshold calculated with the *more realistic* model and with the *more realistic* model without EBEs.

As a matter of a fact, this notion also encompasses the treatment of EBEs that have an energy distribution very different from SEs. We realized another simulation in the *more realistic* configuration, with an EBEEY set to 0. The evolution of the multipactor threshold calculated by POTOMAC is represented in Fig. 15. Removing EBEs increases the multipactor threshold of 5%–27% between 0 and 40 V. For potentials higher than 40 V, it cancels the multipactor. It is due to the fact that, for high potentials, the multipactor appearance involves a lot of very low energy collisions for which the EBEEY is the highest. These results highlight an important point: even in small gap geometries, the velocity spread plays an important role.

We also neglected the influence of the $\mathbf{H}_{\text{RF}}$ field. It tends to push electrons toward the lateral walls of the waveguide (Miller force),[35] creating a spatial instability. As the RF electric field amplitude is lower at the sides of the waveguide, the electrons pushed away from the center go under a weaker acceleration, and their energy is too low to ensure $\sigma > 1$. When the time between the emission and the collision of electrons, called the flight time, is relatively small, neglecting $\mathbf{H}_{\text{RF}}$ is an acceptable hypothesis.[35] This is typically the case when $W \gg d$. However, in our configuration, some multipactor modes involve electrons with an important flight time. We expect that considering $\mathbf{H}_{\text{RF}}$ would slightly raise the multipactor threshold, without fundamentally change the dynamics at stake. A new set of simulations would be required to precisely assert the importance of this hypothesis.

VIII. CONCLUSIONS

In this paper, we led a detailed study of the multipactor appearance in two RF systems holding a potential difference V_d between their plates. The first one was an infinite parallel-plate system, studied in 1D, with a simplified electron emission model. The second

system was a rectangular waveguide, studied in 3D, with a more realistic electron emission model. We calculated the evolution of these systems' multipactor threshold with V_d, with the numerical tool POTOMAC. In the first configuration, we used resonance theory to determine which mode appeared at different potentials and the theoretical threshold of the system. For the two RF systems, POTOMAC simulations outlined an important dependence of the multipactor threshold E_{th} on the potential difference between the plates V_d.

In the parallel-plate system, there was no dispersion in the impact velocities of the electrons, which caused significant and unphysical threshold variations at V_d = 26.5 and 47.0 V. We observed that, when increasing V_d, the multipactor progressively switches from DS ($\Pi = 2\pi, n_\varphi = 2$) dynamics to chaotic multipactor. Then, there is a smooth transition between various asymmetric SS modes. For very high potentials, the multipactor becomes chaotic again. In this same geometry, we computed the theoretical threshold, which matched POTOMAC. Hence, we can validate both POTOMAC and our implementation of resonance theory.

In the rectangular waveguide, the dispersion in electrons impact velocities makes the notion of modes irrelevant. However, we confirmed the assertion of other authors[7] according to whom multipactor progressively switches from DS to SS dynamics. The general shape of the $E_{\text{th}}(V_d)$ curve was similar to that of the parallel plate, at the exception of the unphysical variations of E_{th}. We observed that omitting the EBEs in this configuration led to a premature disappearance of the multipactor (40 V instead of 55 V). It outlines the important dependence of E_{th} not only on the electron emission properties of the walls of the system wall but also on its modeling.

ACKNOWLEDGMENTS

This work was carried out within the framework of the EUROfusion Consortium and received funding from the Euratom Research and Training Programme 2014–2018 and 2019–2020 under Grant Agreement No. 633053. The views and opinions expressed herein do not necessarily reflect those of the European Commission.

AUTHOR DECLARATIONS

Conflict of Interest

The authors have no conflicts to disclose.

DATA AVAILABILITY

Some of the data that support the findings of this study are openly available in Zenodo at http://dx.doi.org/10.5281/zenodo.3648704.[19] The remaining data that support the findings of this study are available from the corresponding author upon reasonable request.

APPENDIX: POTOMAC CONVERGENCE AND CONSISTENCY STUDIES

In their study,[40] Anza *et al.* determined the multipactor threshold of an infinite parallel-plate system. Their study has the merit to compute the threshold of the structure with different methods: statistical theories, PIC simulations, and an experimental study. We led a set of POTOMAC simulations in their configuration: the gap d = 1 mm, and the frequency f = 1.64 GHz. The material is silver, and TEEY is calculated with modified Vaughan model.[20,21,40,41] For this fd product, we can refer to the study of Anza *et al.* (Fig. 11), which states that the voltage threshold is around 100 V; it is consistent with POTOMAC, whose threshold is 104 V in this configuration.

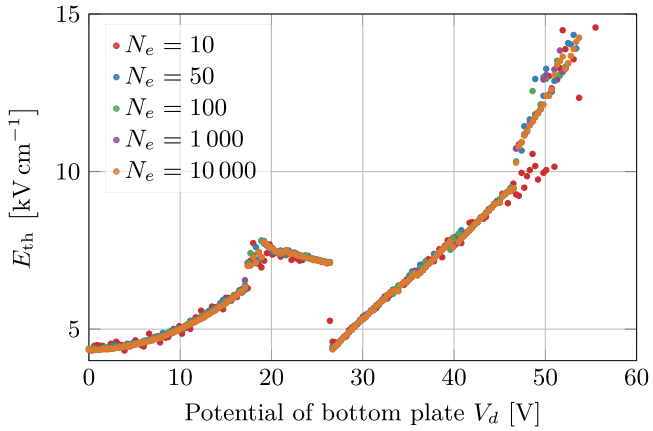

FIG. 16. The evolution of the multipactor threshold with V_d, in the geometry presented in Sec. II and with different values of N_e.

We represented in Fig. 16 the evolution of the multipactor threshold with V_d as calculated by POTOMAC for different numbers of initial electrons. The configuration is the same as in Sec. II, where 100 electrons are enough to ensure convergence. N_e = 100 is also adequate in the configuration discussed in Sec. VI.

REFERENCES

[1] J. R. M. Vaughan, "Multipactor," IEEE Trans. Electron Devices **35**, 1172–1180 (1988).
[2] E. Sorolla, "Contribution to modeling multipactor and corona discharges in high power electromagnetic fields," Ph.D. thesis, École Polytechnique Fédérale de Lausanne, 2012.
[3] V. E. Semenov, N. A. Zharova, N. I. Zaitsev, A. K. Gvozdev, A. A. Sorokin, M. Lisak, J. Rasch, and J. Puech, "Reduction of the multipactor threshold due to electron cyclotron resonance," IEEE Trans. Plasma Sci. **40**, 3062–3069 (2012).
[4] N. Fil, M. Belhaj, J. Hillairet, J. Puech, and R. Mathevet, "Electron emission under uniform magnetic field of materials for fusion and space applications," Fusion Eng. Des. **123**, 426–430 (2017).
[5] N. Balcon, M. Belhaj, T. Tondu, J. C. Mateo-Velez, and D. Payan, "Secondary electron emission of cover glasses: Temperature and incident flux effects," in *International Symposium on Materials in the Space Environment*, edited by L. Ouwehand (ESA Communications, Noordwijk, The Netherlands, 2013).
[6] E. Sorolla, M. Belhaj, J. Sombrin, and J. Puech, "New multipactor dynamics in presence of dielectrics," Phys. Plasmas **24**, 103508 (2017).
[7] Y. Zhai, H. Wang, L. Zhang, S. Lin, Y. Li, and Y. Li, "Effect of secondary emission yield and initial charge of dielectric material on multipactor in parallel-plate dielectric-loaded waveguide," IEEE Trans. Electron Devices **66**, 5333–5338 (2019).
[8] A. Berenguer, Á. Coves, F. Mesa, E. Bronchalo, and B. Gimeno, "Analysis of multipactor effect in a partially dielectric-loaded rectangular waveguide," IEEE Trans. Plasma Sci. **47**, 259 (2018).
[9] N. Fil, M. Belhaj, J. Hillairet, and J. Puech, "Multipactor threshold sensitivity to total electron emission yield in small gap waveguide structure and TEEY models accuracy," Phys. Plasmas **23**, 123118 (2016).

[10]A. Plaçais, M. Belhaj, J. Hillairet, and J. Puech, "A three-dimensional Dionne model for multipactor simulations," Phys. Plasmas **27**, 053512 (2020).
[11]A. Plaçais, E. Sorolla, M. Belhaj, J. Hillairet, and J. Puech, "Influence of work function on the multipactor threshold," in *2018 IEEE MTT-S International Conference on Numerical Electromagnetic and Multiphysics Modeling and Optimization (NEMO)* (IEEE, Reykjavik, Iceland, 2018), pp. 1–4.
[12]A. Plaçais, M. Belhaj, J. Hillairet, and J. Puech, "POTOMAC: Towards a realistic secondary and backscattered emission model for the multipactor," in *2019 IEEE Pulsed Power and Plasma Science (PPPS)* (IEEE, Orlando, 2019), pp. 1–4.
[13]S. Riyopoulos, "Multipactor saturation due to space-charge-induced debunching," Phys. Plasmas **4**, 1448–1462 (1997).
[14]A. Coves, G. Torregrosa-Penalva, C. Vicente, B. Gimeno, and V. E. Boria, "Multipactor discharges in parallel-plate dielectric-loaded waveguides including space-charge effects," IEEE Trans. Electron Devices **55**, 2505–2511 (2008).
[15]L. Brieba, *Plasma Simulations by Example*, 1st ed. (CRC Press, 2019), p. 348.
[16]P. L'Ecuyer, "Maximally equidistributed combined Tausworthe generators," Math. Comput. **65**, 203–214 (1996).
[17]M. A. Furman and M. T. F. Pivi, "Probabilistic model for the simulation of secondary electron emission," Phys. Rev. Spec. Top.–Accel. Beams **5**, 124404 (2002).
[18]M. A. Furman and M. T. F. Pivi, "Erratum: Probabilistic model for the simulation of secondary electron emission [Phys. Rev. ST Accel. Beams 5, 124404 (2002)]," Phys. Rev. Spec. Top.–Accel. Beams **16**, 069901 (2013).
[19]A. Plaçais, M. Belhaj, and S. Dadouch (2020). "ONERA copper TEEY measurements with various surface state and incidence angle," Zenodo. https://doi.org/10.5281/zenodo.3648704
[20]J. R. M. Vaughan, "A new formula for secondary emission yield," IEEE Trans. Electron Devices **36**, 1963–1967 (1989).
[21]R. M. Vaughan, "Secondary emission formulas," IEEE Trans. Electron Devices **40**, 830 (1993).
[22]R. A. Kishek, "Ping-pong modes: A new form of multipactor," Phys. Rev. Lett. **108**, 035003 (2012).
[23]K. G. Mckay, "Secondary electron emission," Adv. Electron. Electron Phys. **1**, 65–130 (1948).
[24]S. Riyopoulos, D. Chernin, and D. Dialetis, "Effect of random secondary delay times and emission velocities in electron multipactors," IEEE Trans. Electron Devices **44**, 489–497 (1997).
[25]E. W. B. Gill and A. von Engel, "Starting potentials of high-frequency gas discharges at low pressure," Proc. R. Soc. London, Ser. A **192**, 446–463 (1948).
[26]S. Riyopoulos, "Higher-order, asymmetric orbit multipactors," Phys. Plasmas **14**, 112101 (2007).
[27]R. A. Kishek, "Coexistence of mixed mode multipactor," Phys. Plasmas **19**, 124501 (2012).
[28]R. A. Kishek, "Bifurcation and period-n multipactor," in MULCOPIM, Valencia, Spain, 2014.
[29]M. A. Branch, T. F. Coleman, and Y. Li, "A Subspace, Interior, and conjugate gradient method for large-scale bound-constrained minimization problems," SIAM J. Sci. Comput. **21**, 1–23 (1999).
[30]The SciPy Community, SciPy v1.5.3 Reference Guide, 2020.
[31]M. Mostajeran and M. Lamehi Rachti, "On the phase stability in two-sided multipactor," Nucl. Instrum. Methods Phys. Res., Sect. A **615**, 1–5 (2010).
[32]M. Mostajeran, "Can accurate investigation of phase stability explain the experimental results of multipactor phenomenon?," J. Instrum. **8**, P04027 (2013).
[33]A. Kryazhev, M. Buyanova, V. Semenov, D. Anderson, M. Lisak, J. Puech, L. Lapierre, and J. Sombrin, "Hybrid resonant modes of two-sided multipactor and transition to the polyphase regime," Phys. Plasmas **9**, 4736–4743 (2002).
[34]V. Semenov, V. Nechaev, E. Rakova, N. Zharova, D. Anderson, M. Lisak, and J. Puech, "Multiphase regimes of single-surface multipactor," Phys. Plasmas **12**, 073508 (2005).
[35]V. E. Semenov, E. I. Rakova, D. Anderson, M. Lisak, and J. Puech, "Multipactor in rectangular waveguides," Phys. Plasmas **14**, 033501 (2007).
[36]J. Greenwood, "The correct and incorrect generation of a cosine distribution of scattered particles for Monte-Carlo modelling of vacuum systems," Vacuum **67**, 217–222 (2002).
[37]M. S. Chung and T. E. Everhart, "Simple calculation of energy distribution of low-energy secondary electrons emitted from metals under electron bombardment," J. Appl. Phys. **45**, 707–709 (1974).
[38]A. Jablonski, P. Mrozek, G. Gergely, M. Menhyárd, and A. Sulyok, "The inelastic mean free path of electrons in some semiconductor compounds and metals," Surf. Interface Anal. **6**, 291–294 (1984).
[39]J. Rasch and J. F. Johansson, "Non-resonant multipactor—A statistical model," Phys. Plasmas **19**, 123505 (2012).
[40]S. Anza, C. Vicente, J. Gil, V. E. Boria, B. Gimeno, and D. Raboso, "Nonstationary statistical theory for multipactor," Phys. Plasmas **17**, 062110 (2010).
[41]C. P. Vicente, M. Mattes, D. Wolk, H. Hartnagel, J. R. Mosig, and D. Raboso, "FEST3D—A simulation tool for multipactor prediction," *MULCOPIM* (Noordwijk, The Netherlands, 2005), p. 16827.